Turkish Journal of Electrical Engineering & Computer Sciences

http://journals.tubitak.gov.tr/elektrik/

Research Article

Turk J Elec Eng & Comp Sci
(2016) 24: 2174 – 2193

doi:10.3906/elk-1402-87

Dynamic analysis of a modular isolated bidirectional dc-dc converter for high power applications

Farzad SEDAGHATI[1], **Seyed Hossein HOSSEINI**[1,*], **Mehran SABAHI**[1], **Gevorg BABAMALEK GHAREHPETIAN**[2]

[1]Faculty of Electrical and Computer Engineering, University of Tabriz, Tabriz, Iran
[2]Electrical Engineering Department, Amirkabir University of Technology, Tehran, Iran

Received: 10.02.2014 • **Accepted/Published Online:** 05.07.2014 • **Final Version:** 15.04.2016

Abstract: A new configuration for modular isolated bidirectional dc-dc converters is presented. The proposed converter has interesting features such as fewer switching devices, bidirectional power flow, and low switching losses. The simple modular structure, high frequency operation, zero voltage switching (ZVS) capability, and fewer switching devices make the extended configuration of the proposed converter suitable for high power applications. The operation principle of the proposed converter is analyzed in steady state, and then ZVS analysis of the converter is presented in detail. A generalized averaging technique, which uses dc and first order terms of Fourier's series of state variables, is applied to model the converter. A small-signal average model is developed to obtain the control-to-output transfer function of the converter. In order to obtain acceptable dynamic response, closed-loop control of the converter using a PID controller is studied. Finally, measurement and simulation results are presented to verify the operation principles of the converter and effectiveness of the PID controller.

Key words: Modular converter, isolated dc-dc converter, bidirectional power flow, generalized average modeling.

1. Introduction

The integration of modular power converters enables low rating components to be used in high power applications. Modular power conversion systems, with series or parallel converter modules at output and input sides, are classified into four architectures considering their connection forms, namely, input-series output-series (ISOS), input-series output-parallel (ISOP), input-parallel output-series (IPOS), and input-parallel output-parallel (IPOP). The advantages of modular conversion systems include ease of thermal design, each module handles only a part of the total power, straightforward design process, increased system reliability due to reduced thermal and electrical stresses on power switches and components, improved system reliability due to redundancy, lowered cost and ease of expansion, and therefore step by step increase of the system rating [1,2].

Several modular isolated bidirectional dc-dc converters have been reported in the literature [3–11]. Most of them have been designed for a specific application and some of them have focused on developing control techniques to achieve equal input voltage and output current sharing and improve the dynamic performance. Based on the proposed research review, it can be said that most of the modular isolated bidirectional dc-dc converters have used a dual active bridge (DAB) dc-dc converter as a basic module. The bidirectional isolated DAB dc-dc converter, initially presented in [12,13], is considered as a suitable case for medium and high power

*Correspondence: hosseini@tabrizu.ac.ir

applications. This converter has many advantages such as electrical isolation, high reliability, soft-switching capability, and bidirectional power flow [12,13]. However, employment of the DAB dc-dc converter as a basic module results in a high number of power switching devices, high cost, and large size of modular converter. Therefore, the expansion of the converter is very limited for high power applications. In some cases, a dual half bridge (DHB) dc-dc converter has been used as a basic module. The DHB topology uses only half as many switching devices as the DAB topology [14,15]. However, the main drawback of DHB topology is that the split dc-link capacitors have to withstand the full load current. Hence, the DHB converter is suitable for low power applications [14]. Therefore, this solution reduces power transfer capacity and needs switches with higher ratings.

A closed-loop controller is needed to regulate the output of a dc-dc converter. The design of the controller requires a small-signal average model of the converter. State-space averaging is a common technique to model switching converters. This technique has been applied to model the single-phase DAB dc-dc converter [16–18] and three-phase dc-dc converters [19,20]. The conventional averaging techniques for modeling dc-dc converters neglect the current ripple [21], but this assumption is not acceptable for a converter with a high frequency isolating transformer because the current of the transformer is purely ac. A generalized averaging technique, which represents state variables using more coefficients of Fourier's series, can be used to model the converter with a high frequency isolating transformer. This technique has been used to model the single-phase ac-dc converter [22] and dc-ac resonant converter [23]. Moreover, this averaging technique has been applied to the DAB dc-dc converter [24].

This paper proposes a new topology for modular isolated bidirectional dc-dc converters using fewer switching devices, to reduce the cost and size without imposing any limitation on the converter power rating. The proposed converter has bidirectional power flow capability. In addition, it has the capability of easy expansion for high power applications. Based on two later capabilities, the application of "a connection between two dc-links with different nominal voltage in a dc microgrid" is proposed for the converter. Dynamic analysis based on generalized averaging technique is presented and closed-loop control of the converter using a PID controller is studied. The simulation and measurement results are provided to confirm the theoretical aspects of the controller and the proposed converter.

2. Configuration and operation principles of the proposed converter

2.1. Configuration

Figure 1 shows the proposed modular isolated bidirectional dc-dc converter, with N modules, and parallel or cascaded connection of high frequency transformer windings and power switches. The converter's modular bridges are the generalized forms of the conventional full-bridge.

As shown in Figure 1, basic modules of bridges contain one of the transformer windings and two power switches connected to the ends of the winding. The modular parallel bridge is based on the parallel connection of modules, and each of two adjacent parallel modules has reverse directions of magnetic flux. The modular series bridge is a cascaded connection of modules, and each of two adjacent cascaded modules has reverse directions of magnetic flux. In this configuration, the switches that are placed between each pair of windings are named inner switches, and the other four switches, which are proprietary of the first and the last windings, are named outer switches.

Series or parallel connection of modules is selected considering the requirements of converter voltage and current ratings. Using the proposed modular parallel and series bridges, all four possible architectures of

modular converter (i.e., IPOS, IPOP, ISOP, and ISOS) are achievable. This work focuses on the IPOS modular isolated bidirectional dc-dc converter architecture, which can be employed for power transmission between two high power and high voltage dc-links. As shown in Figure 1, the primary or low voltage side of the proposed IPOS converter consists of a low voltage dc-link and modular parallel bridge. The secondary or high voltage side of the converter consists of a high voltage dc-link and modular series bridge. High frequency transformers are applied to transmit power and perform a galvanic isolation between two sides. Primary windings of transformers are placed in the primary side bridge, and secondary windings are placed in the secondary side bridge. In each module, the sum of the transformer leakage inductance and external auxiliary inductance is considered as an equivalent inductance in the secondary side of the transformer.

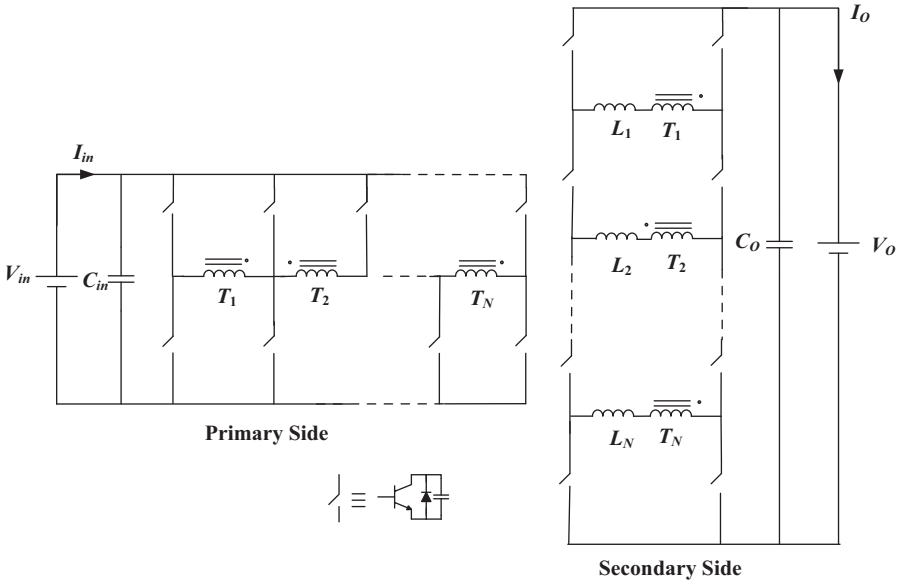

Figure 1. Proposed IPOS modular isolated bidirectional dc-dc converter.

2.2. Analysis of operation principles

Figures 2a and 2b show the switching operation of the proposed IPOS converter with two modules during one switching cycle. To generate a high frequency ac voltage on transformer windings, in the parallel bridge, three

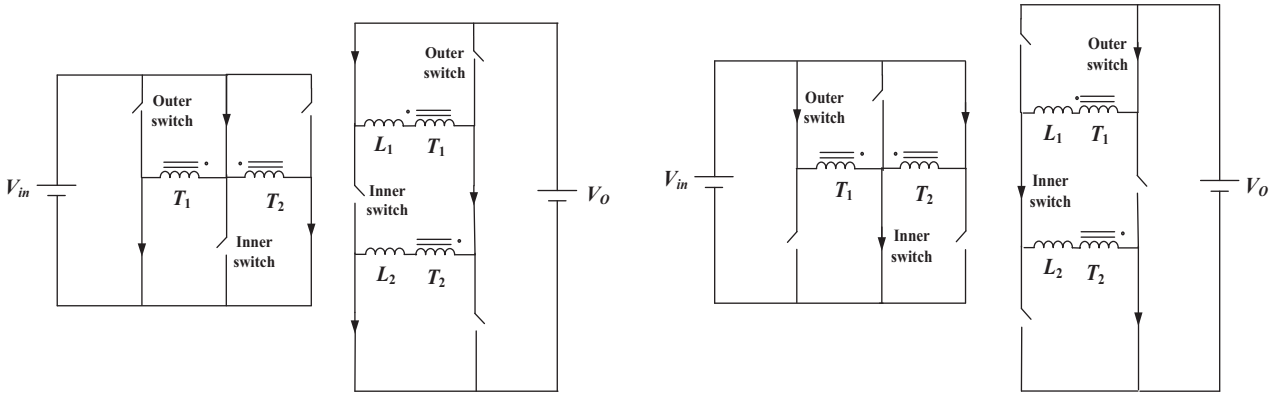

Figure 2. Switching operation of proposed IPOS converter with two modules during one switching cycle, in (a) first and (b) second half cycle.

switches conduct the current in each half cycle, one inner switch in one step, and two outer switches in the other step; and in the series bridge, one inner switch in one of the bridge legs, and two outer switches in the other leg conduct the current in each half cycle.

Using a phase shift control algorithm, the first bridge provides square wave voltage with a duty ratio of 50% to the primary winding of the transformer in each module, and the square wave voltage of the secondary winding has a finite phase shift from the primary one in order to transfer power from the primary side to the secondary side. The leakage inductance of transformers and external auxiliary inductors serve as instantaneous energy storage components. Figure 3a illustrates the process of power transfer from the primary to the secondary side. The phase shift angle is defined to be positive in this power transfer process, which means that the primary side phase is leading the secondary side phase. The proposed converter has the capability of bidirectional power flow. As shown in Figure 3b, when the secondary side phase is leading the primary side phase, power is transmitted from the secondary to the primary. In this condition, the phase shift angle is defined to be negative.

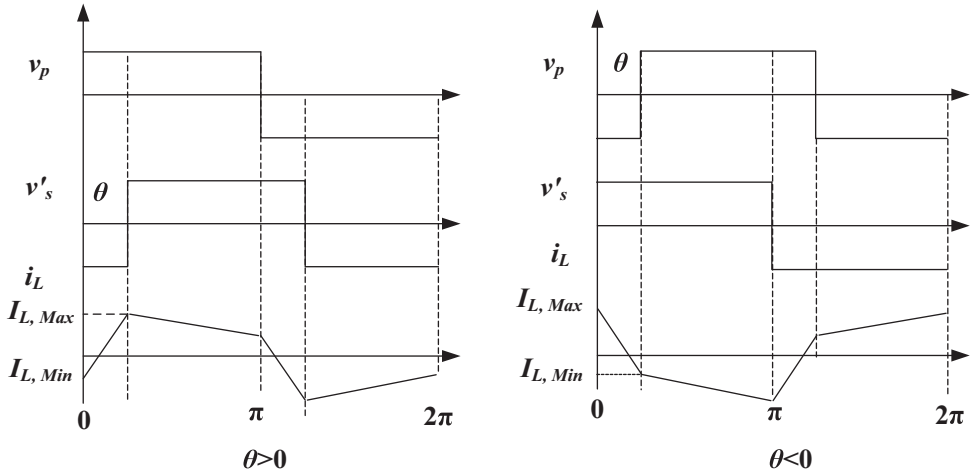

Figure 3. Transformer voltages and current during one switching cycle, when $v_p = nv_s$, for power transmission (a) from primary to secondary and (b) from secondary to primary.

Considering Figure 3a, the converter average input current for each module over one switching cycle is determined as follows [25]:

$$\bar{i}_{in} = \frac{V_O^{'}}{L\omega}\theta(1 - \frac{\theta}{\pi}), \tag{1}$$

where L is the sum of each transformer leakage inductance referred to primary and external auxiliary inductor. ω is the switching frequency in radians per second. Moreover, $n(= n_1/n_2)$ is defined as the transformer turns ratio, and θ is the phase shift angle between the voltage of two bridges in radians. V_{in} and V_O are defined as modular converter input and output dc voltages, and $V_O^{'}$ is the output dc voltage referred to primary, i.e. $(nV_O)/N$.

Notice that in steady state the transformer current is symmetrical for each half switching cycle; therefore, $i_L(0) = -i_L(\pi)$. If the losses of a converter are negligible, then the output power is equal to the input power. Therefore, the amount of power transmitted to the load via each module is calculated as follows:

$$P = \frac{V_{in}V_O^{'}}{L\omega}\theta(1 - \frac{\theta}{\pi}) = \frac{nV_{in}V_O}{NL\omega}\theta(1 - \frac{\theta}{\pi}) \tag{2}$$

and the total output power of the proposed IPOS converter with N modules is determined as follows:

$$P_t = N \times P = N\frac{nV_{in}V_O}{NL\omega}\theta(1-\frac{\theta}{\pi}) = \frac{nV_{in}V_O}{L\omega}\theta(1-\frac{\theta}{\pi}) \tag{3}$$

3. ZVS operation analysis of the proposed converter

In the proposed converter, a snubber capacitor is paralleled with each switch to reduce the switching losses and damp out overvoltages. However, if each switch is turned on with the charged snubber capacitor, the switch shorts out the capacitor and dissipates the stored energy [26]. Therefore, it is necessary to provide the ZVS condition for the switches. Each switch can be turned on in ZVS condition, when $V_1/n = V_2/N$ and, moreover, the power transfer is sufficient. When $V_1/n \neq V_2/N$, the switch is not necessarily turned on in ZVS condition. Figure 4 shows ZVS operation of the secondary side bridge. In the secondary side bridge, switching maximum and minimum currents are defined as stated in (4) and (5)

$$I_{L,Min} = -\frac{[(V_1/n)+(V_2/N)]\theta + [(V_1/n)-(V_2/N)](\pi-\theta)}{2L\omega} \tag{4}$$

$$I_{L,Max} = \frac{[(V_1/n)+(V_2/N)]\theta - [(V_1/n)-(V_2/N)](\pi-\theta)}{2L\omega} \tag{5}$$

As shown in Figure 4, the current of i_L is flowing in switch S_3, and after turning off of switch S_3, the dead time starts. The current flowing in switch S_3 is commutated to C_{S1}, C_{S3}, and C_{S5}. A resonance begins among L and C_{S1}, C_{S3}, and C_{S5}. Capacitor C_{S1} discharges from V_2/N to zero, while C_{S3} charges from zero to $2V_2/N$. When C_{S1} discharges down to zero, the current is commutated to diode D_1. Generating a gating signal during conduction of diode D_1 makes S_1 ready to conduct the current. Switch S_1 starts to conduct the current after the current of diode D_1 decays to zero and changes its polarity. ZVS operation of switches is provided when the following equation is satis?ed:

$$I_{L,Min} < 0 \Rightarrow \theta \geq \frac{V_2 - NV_1/n}{2V_2}\pi \tag{6}$$

Besides the above criterion, if the energy for charging and discharging of snubber capacitors is not sufficient, despite the switching minimum current being negative, the switches cannot be turned on in ZVS condition. Suppose that at $t=0$ switch S_3 turns off and none of the devices are conducting. Once the device turns off, the current in L discharges C_{S1} and charges C_{S3} in the resonant manner until their respective voltages reach the opposite values. If in this instant the current is still positive, diode D_1 turns on and clamps the voltage across C_{S1} to zero and C_{S3} to $2V_2/N$. Now the minimum value of the current i_L at $t=0$, which ensures that the voltage across switch S_3 reaches the clamping value when current i_L reaches zero, is determined. The input bridge is replaced by the secondary-referred voltage source as V_1/n, with the polarity required during this event. The time $t = t_m$ is defined as the instant at which i_L just reaches zero. At time $t=0$, we have $i_L = I_{L,Min}$, $V_{CS1} = V_2/N$, $V_{CS3} = 0$ and at time $t= t_m$, we have $i_L = 0$, $V_{CS1} = 0$, $V_{CS3} = 2V_2/N$. During the interval $0 < t < t_m$, we have

$$i_L = i_{C_{S1}} + i_{C_{S3}} \tag{7}$$

$$i_L = C_{S1}\frac{dv_{C_{S1}}}{dt} - C_{S3}\frac{dv_{C_{S3}}}{dt} = C_{S1}\frac{dv_{C_{S1}}}{dt} - (-2C_{S1}\frac{dv_{C_{S1}}}{dt}) \tag{8}$$

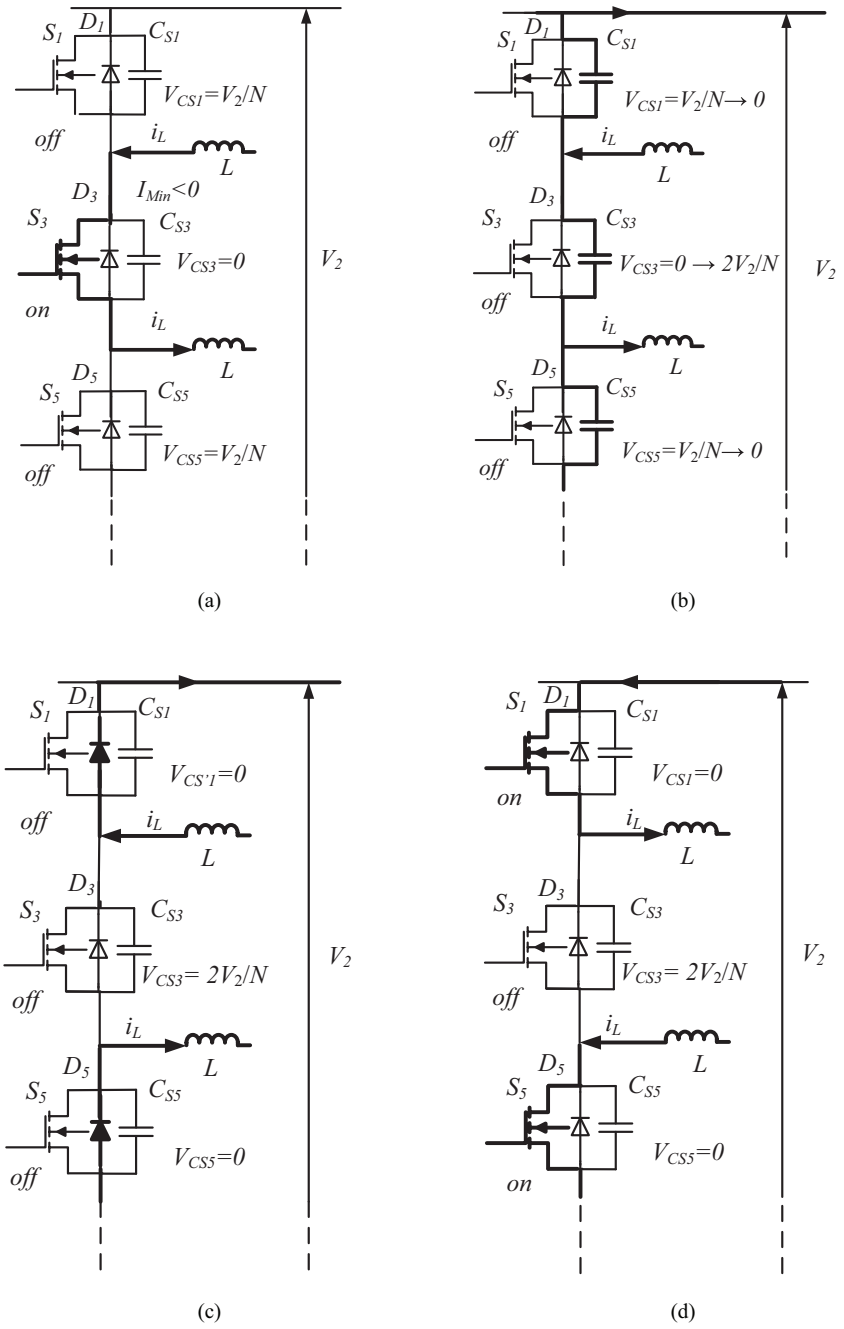

Figure 4. ZVS operation of the proposed converter, (a) just before dead time starts, (b) just after dead time starts, (c) diode freewheeling, and (d) current polarity change after the dead time.

$$i_L = 3C_{S1}\frac{dv_{C_{S1}}}{dt} = 3C\frac{dv_C}{dt} \tag{9}$$

The energy balance indicates that $E_{(t=0)} = E_{(t=tm)} + E_{Losses} + E_{Delivered}$, and based on the assumption of lossless circuit, we have $E_{(t=0)} - E_{(t=tm)} = E_{Delivered}$; thus, the following equation is achieved:

$$2 \times \frac{1}{2} L I_{L,Min}^2 = E_{Delivered} \tag{10}$$

To reach the ZVS condition, $E_{Delivered}$ should be equal to

$$E_{Delivered} = \int_0^{t_m} i_L (V_1/n) dt = \int_0^{t_m} 3C \frac{dV_C}{dt} (V_1/n) dt = 6CV_1V_2/(nN) \tag{11}$$

Using (10) and (11), the minimum current of the bridge is derived as follows:

$$|I_{L,Min}| \geq \sqrt{6} \sqrt{\frac{C}{L}} \sqrt{\frac{V_1 V_2}{nN}} \tag{12}$$

If similar analysis is used for the four marginal switches in the bridge, the following inequality is achieved. Notice that (12) is valid for the rest of the switches.

$$|I_{L,Min}| \geq 2 \sqrt{\frac{C}{L}} \sqrt{\frac{V_1 V_2}{nN}} \tag{13}$$

Similar analysis can be considered for the parallel bridge.

4. Modeling and control of proposed converter

4.1. Small-signal model

In the modeling, it is assumed that the transformer magnetizing current and voltage drop across the switch are not significant, and switching transients are negligible. The input capacitance is relatively large and so its dynamics are not considered in the modeling. Figure 5 shows the simplified model of the proposed modular converter. The current source on the output may have either polarity for bidirectional power flow [24]. The sum of the transformer leakage inductance and that of the auxiliary inductor in the jth module is defined as module inductance, L_j, which is referred to the output side. Similarly, switch on-time resistance and transformer winding resistance in the jth module are defined as module resistance, R_j. For the sake of simplicity, the transformers turn ratios are selected to be unity ($n = 1$).

The phase shift modulation results in this point that the voltage at the primary side of jth transformer, v_{pj}, can only have two states, namely, $+V_{in}$, when the switches $S_{2j-1,1}$ and $S_{2j+1,1}$ are ON, and $-V_{in}$, when the switches $S_{2j,1}$ and $S_{2j+2,1}$ are ON. Thus, the input voltages of transformers are defined as follows:

$$v_{pj}(\tau) = U_1(\tau) v_{in}(\tau) \;\; ; \quad j = \;\; 1 \quad \text{to} \quad \; N \;\; , \tag{14}$$

where the switching function of the input bridge, $U_1(\tau)$, is considered as follows [24]:

$$U_1(\tau) = \begin{cases} 1 & 0 \leq \tau < \frac{T}{2} \\ -1 & \frac{T}{2} \leq \tau < T \end{cases} \;\; , \tag{15}$$

where $T = 2\pi/\omega$. In this analysis, τ denotes the time within a period referenced to the rising edge of U_1. In a similar way, for the output voltage of transformers, we have

$$\sum_{j=1}^{N} v_{sj}(\tau) = U_2(\tau) v_O(\tau), \tag{16}$$

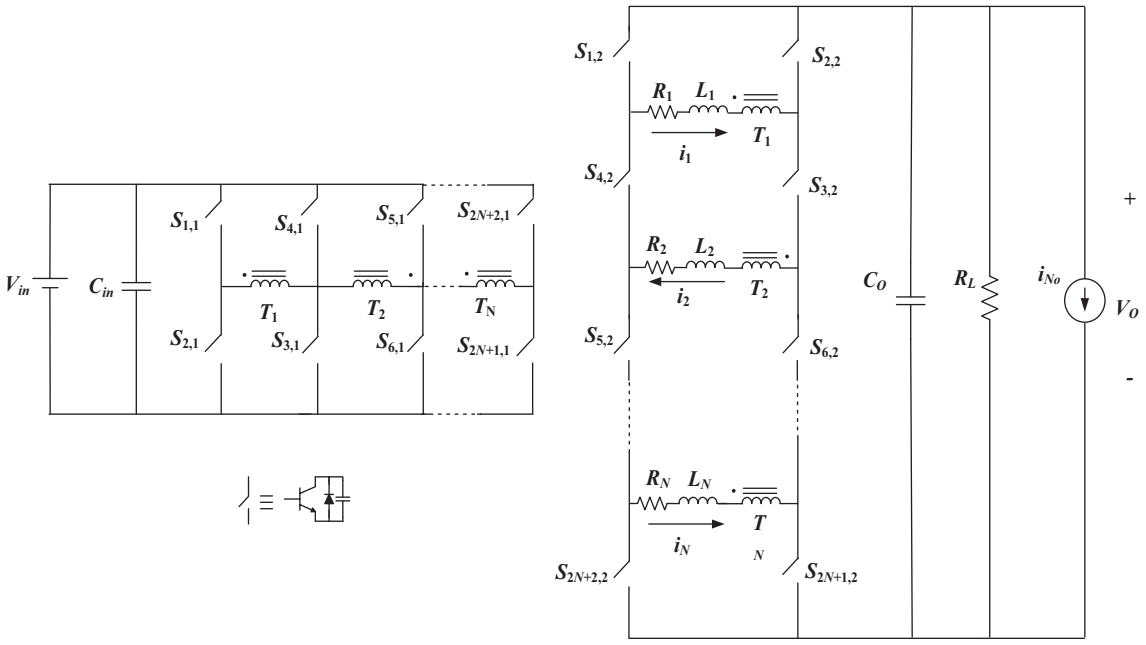

Figure 5. Simplified model of proposed converter.

where the switching function of the output bridge, $U_2(\tau)$, is considered as follows:

$$U_2(\tau) = \begin{cases} 1 & \frac{\phi T}{2} \le \tau < \frac{\phi T}{2} + \frac{T}{2} \\ -1 & 0 \le \tau < \frac{\phi T}{2} \quad \text{and} \quad \frac{\phi T}{2} + \frac{T}{2} \le \tau < T \end{cases} \tag{17}$$

In the above equation, φ is defined as the phase shift ratio, which is equal to θ/π. As can be seen in Figure 5, the secondary sides of transformers are connected in series and so the total equivalent resistance and total equivalent inductance in the secondary side bridge are calculated as follows:

$$R_{eq} = \sum_{j=1}^{N} R_j \quad ; \quad L_{eq} = \sum_{j=1}^{N} L_j \tag{18}$$

If transformer current, i_L, and output capacitor voltage, v_O, are selected as state variables, then state equations of the proposed converter are derived, as follows:

$$\frac{dv_O(\tau)}{dt} = -\frac{1}{R_L C_O} v_O(\tau) + \frac{1}{C_O} U_2(\tau) i_L(\tau) - \frac{i_{No}}{C_O} \tag{19}$$

$$\frac{di_L(\tau)}{dt} = -\frac{R_{eq}}{L_{eq}} i_L(\tau) + \frac{N}{L_{eq}} U_1(\tau) v_{in}(\tau) - \frac{1}{L_{eq}} U_2(\tau) v_O(\tau) \tag{20}$$

Both equations are time-variant and nonlinear. It is necessary to apply averaging to derive a linear time-invariant model. The conventional state-space averaging technique is applied when the ripples in state variables are small, i.e. considering only dc terms. However, transformer currents in the proposed converter are pure ac currents, which means that the ripple is large and dc coefficient is zero. Therefore, a generalized averaging

technique is applied to model the proposed modular converter. In this technique, state variables are represented using their Fourier's series. In this paper, dc and first order terms of Fourier's series have been used to represent the average of state variables.

It is assumed that the dynamics of the input voltage and load are much slower than those of the converter. Therefore, for dc and first order coefficients of these parameters, we have $\langle v_{in}\rangle_0 = V_{in}; \langle v_{in}\rangle_{1R} = \langle v_{in}\rangle_{1I} = 0$ and $\langle i_{No}\rangle_0 = I_{No}; \langle i_{No}\rangle_{1R} = \langle i_{No}\rangle_{1I} = 0$, where subscripts R and I denote real and imaginary parts of a complex number, respectively. The dc and first order coefficients of state variables and switching functions in (19) and (20) are calculated according to [27,28], and finally the following state-space representation can be written:

$$\frac{d}{dt}\begin{bmatrix} v_{O0} \\ i_{L1R} \\ i_{L1I} \\ i_{L0} \\ v_{O1R} \\ v_{O1I} \end{bmatrix} = \begin{bmatrix} -\frac{1}{R_L C_O} & \frac{-4\sin\phi\pi}{\pi C_O} & \frac{-4\cos\phi\pi}{\pi C_O} & 0 & 0 & 0 \\ \frac{2\sin\phi\pi}{\pi L_{eq}} & -\frac{R_{eq}}{L_{eq}} & \omega & 0 & 0 & 0 \\ \frac{2\cos\phi\pi}{\pi L_{eq}} & -\omega & -\frac{R_{eq}}{L_{eq}} & 0 & 0 & 0 \\ 0 & 0 & 0 & -\frac{R_{eq}}{L_{eq}} & -\frac{4\sin\phi\pi}{\pi L_{eq}} & -\frac{4\cos\phi\pi}{\pi L_{eq}} \\ 0 & 0 & 0 & \frac{-2\sin\phi\pi}{\pi C_O} & -\frac{1}{R_L C_O} & \omega \\ 0 & 0 & 0 & \frac{-2\cos\phi\pi}{\pi C_O} & -\omega & -\frac{1}{R_L C_O} \end{bmatrix} \begin{bmatrix} v_{O0} \\ i_{L1R} \\ i_{L1I} \\ i_{L0} \\ v_{O1R} \\ v_{O1I} \end{bmatrix} + \begin{bmatrix} 0 & -\frac{1}{C_O} \\ 0 & 0 \\ -\frac{2N}{\pi L_{eq}} & 0 \\ 0 & 0 \\ 0 & 0 \\ 0 & 0 \end{bmatrix} \begin{bmatrix} V_{in} \\ I_{No} \end{bmatrix} \tag{21}$$

In the above equation, i_{L0}, v_{O1R}, and v_{O1I} are all zero, if their initial values are zero. Therefore, the dynamics of i_{L0}, v_{O1R}, and v_{O1I} can be decoupled. Thus, the state-space representation of (21) can be reduced to (22).

$$\frac{d}{dt}\begin{bmatrix} v_{O0} \\ i_{L1R} \\ i_{L1I} \end{bmatrix} = \begin{bmatrix} -\frac{1}{R_L C_O} & \frac{-4\sin\phi\pi}{\pi C_O} & \frac{-4\cos\phi\pi}{\pi C_O} \\ \frac{2\sin\phi\pi}{\pi L_{eq}} & -\frac{R_{eq}}{L_{eq}} & \omega \\ \frac{2\cos\phi\pi}{\pi L_{eq}} & -\omega & -\frac{R_{eq}}{L_{eq}} \end{bmatrix} \begin{bmatrix} v_{O0} \\ i_{L1R} \\ i_{L1I} \end{bmatrix} + \begin{bmatrix} 0 & -\frac{1}{C_O} \\ 0 & 0 \\ -\frac{2N}{\pi L_{eq}} & 0 \end{bmatrix} \begin{bmatrix} V_{in} \\ I_{No} \end{bmatrix} \tag{22}$$

This equation illustrates that the dynamic of the proposed modular isolated bidirectional dc-dc converter can be represented using the dc term of the output voltage and first order terms of transformer current. In the above analysis, the effect of the output capacitor equivalent series resistance (ESR) has not been considered, because its consideration results in a coupling among all six state variables and the order of the system would be 6, which has a complicated controller design procedure.

The small-signal control-to-output transfer function should be used to design a controller for the converter. This function describes the dynamic response of the converter against a small perturbation in control signal, φ. For a small perturbation in φ, the state variables v_{O0}, i_{L1R}, and i_{L1I} in (22) will deviate from their steady

state values. Therefore, the control signal and state variables contain two components, namely, steady state value (Φ, V_{O0}, I_{L1R},I_{L1I}) and small-signal ($\Delta\varphi$, Δv_{O0}, Δi_{L1R}, Δi_{L1I}):

$$\phi = \Phi + \Delta\phi; \quad v_{O0} = V_{O0} + \Delta v_{O0}; \quad i_{L1R} = I_{L1R} + \Delta i_{L1R}; \quad i_{L1I} = I_{L1I} + \Delta i_{L1I} \tag{23}$$

Eq. (22) includes the multiplication of the control signal and state variables. For a small $\Delta\varphi$, by approximating nonlinear terms and determining the steady state values of v_{O0}, i_{L1R}, and i_{L1I}, the matrix form of the small-signal model of the proposed converter is achieved as given in (24) and (25).

$$\begin{aligned} \dot{x} &= Ax + Bu \\ y &= Cx + Du \end{aligned} \tag{24}$$

$$x = \begin{bmatrix} \Delta v_{O0} \\ \Delta i_{L1R} \\ \Delta i_{L1I} \end{bmatrix}, \quad A = \begin{bmatrix} -\frac{1}{R_L C_O} & \frac{-4\sin(\Phi\pi)}{\pi C_O} & \frac{-4\cos(\Phi\pi)}{\pi C_O} \\ \frac{2\sin(\Phi\pi)}{\pi L_{eq}} & -\frac{R_{eq}}{L_{eq}} & \omega \\ \frac{2\cos(\Phi\pi)}{\pi L_{eq}} & -\omega & -\frac{R_{eq}}{L_{eq}} \end{bmatrix}; \quad B = \begin{bmatrix} \frac{4}{C_O}[I_{L1I}\sin(\pi\Phi) - I_{L1R}\cos(\pi\Phi)] \\ \frac{2}{L_{eq}} V_{O0}\cos(\pi\Phi) \\ -\frac{2}{L_{eq}} V_{O0}\sin(\pi\Phi) \end{bmatrix}$$

$$y = \Delta v_{O0}, \quad C = [\ 1 \quad 0 \quad 0\ ], \quad D = [0], \quad u = \Delta\phi \tag{25}$$

The control-to-output transfer function is derived to study the effect of operating points and circuit components on the power stage. The frequency response, and transient and steady state responses of the converter are also determined using this transfer function. For the proposed modular converter, the control-to-output transfer function is determined using the small-signal model as follows:

$$G_{v\varphi}(s) = \frac{\Delta v_{O0}}{\Delta\varphi} = C(sI - A)^{-1}B + D \tag{26}$$

By substituting of (25) into (26), the following transfer function is achieved:

$$G_{v\varphi}(s) = \frac{(I_{L1I}\sin(\pi\Phi) - I_{L1R}\cos(\pi\Phi))(\frac{4}{C_O}s^2 + \frac{8R_{eq}}{L_{eq}C_O}s + \frac{4R_{eq}^2}{C_O L_{eq}^2} + \frac{4\omega^2}{C_O}) + \frac{8V_{O0}\omega}{L_{eq}\pi C_O}}{s^3 + (\frac{2R_{eq}}{L_{eq}} + \frac{1}{R_L C_O})s^2 + (\frac{R_{eq}^2}{L_{eq}^2} + \frac{2R_{eq}}{R_L L_{eq} C_O} + \omega^2 + \frac{8}{\pi^2 L_{eq} C_O})s + \frac{1}{R_L C_O}(\frac{R_{eq}^2}{L_{eq}^2} + \omega^2) + \frac{8R_{eq}}{\pi^2 L_{eq}^2 C_O}} \tag{27}$$

Figures 6a, 6b, and 6c show the Bode diagram, root locus, and unit-step response of the above control-to-output voltage transfer function for the parameters given in Table 1, respectively. The phase margin of the open-loop system is equal to –78°. It is obvious that the transfer function is unstable (because of a pair of right half zone poles), and also the low frequency gain is not adequate for the output dc voltage regulation. Therefore, it is necessary to design a proper controller in order to use the converter as a stable system with acceptable transient and steady state responses.

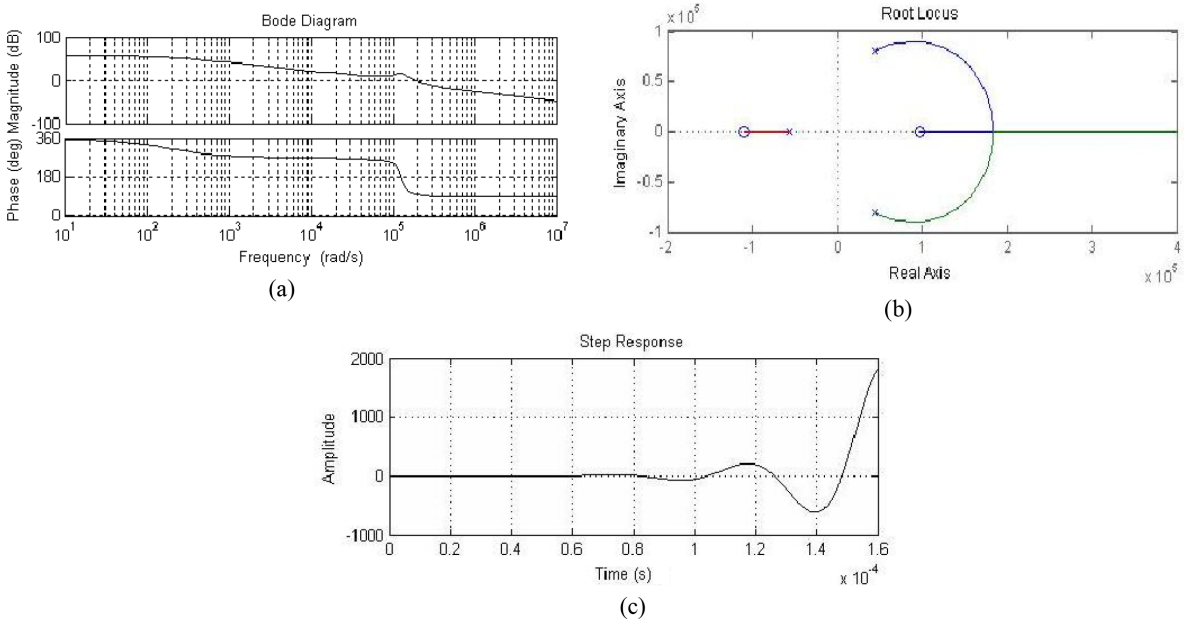

Figure 6. Control-to-output transfer function (a) Bode diagram, (b) Root Locus and (c) unit-step response.

Table 1. Parameters of simulated converter.

Number of modules	2
Input voltage	100 V
Output voltage	200 V
Output power	2 kW
Switching frequency	20 kHz
Turn ratio of transformers (n_2:n_1)	50:50
Total leakage inductance	40 μH

4.2. Controller design

A PD controller may be applied to increase the stability margin and improve the transient response. Moreover, a PI controller is suggested to improve the steady state response. The advantages of PD and PI controllers can be combined to obtain a wide bandwidth and zero steady state error. Therefore, a PID controller with the following transfer function is designed and employed for the proposed converter, as shown in Figure 7a.

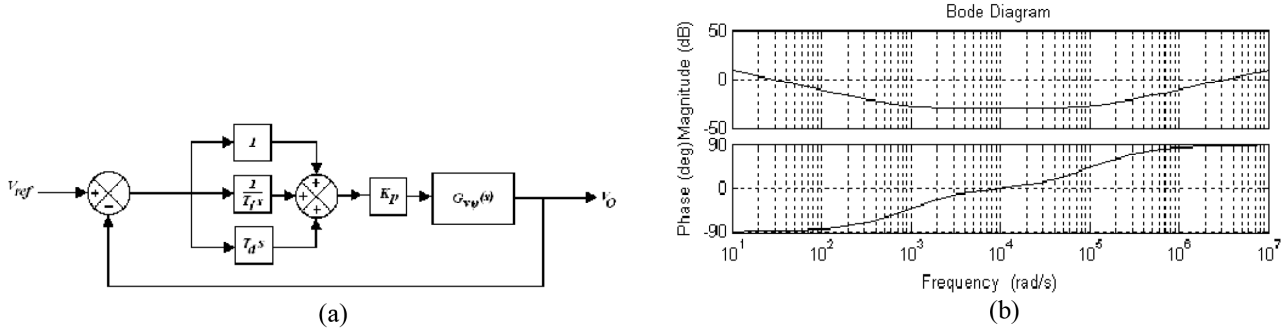

Figure 7. (a) Closed-loop block diagram of controlled converter with PID controller, (b) Bode diagram of the designed PID controller.

$$G_{con}(s) = K_P(1 + \frac{1}{T_i s} + T_d s) \tag{28}$$

The PID controller is designed using a computational optimization approach [29]. It is desired to find a combination of PID controller parameters, i.e. K_p, T_i, and T_d, such that the closed-loop system has desired maximum overshoot and settling time in the unit-step response. There may be more than one set of parameters that satisfy the specifications. To solve this problem, it is necessary to specify the region to search for appropriate parameters K_p, T_i, and T_d. Then a program is written that, in the unit-step response, a combination of parameters is found that will satisfy the criteria of the maximum overshoot and settling time. If a solution does not exist in this region, then it is needed to expand it. In the computational approach, it is necessary to determine the step size for each of parameters K_p, T_i, and T_d region. In the actual design process, it is needed to choose step sizes small enough. In this paper, the object is to find a combination of parameter values such that the closed-loop system has a maximum overshoot of less than 12%, but more than 10%, in the unit-step response. In addition, the settling time should be less than 3 *ms*. The selected combination of parameters for the controller are listed in Table 2. Figure 7b shows the Bode diagram of the designed PID controller. Figure 8a shows the Bode diagram of the open-loop transfer function of the compensated system. In comparison with the uncompensated system, the controller increases the low frequency loop gain and causes a better regulation of the output voltage. The phase margin of the compensated system is increased to 75°. In addition, Figure 8b illustrates the root locus of the system open-loop gain when the effect of the PID controller is considered. This figure indicates that the controller increases the stability margin. Figure 8c shows the unit-step response of the closed-loop transfer function of the compensated system, presenting important information about transient and steady state operations. The unit-step response overshoot is equal to 10.3% and settling time is equal to 2.9 *ms*. Therefore, the controller shows an acceptable operation from stability, steady state, and transient responses point of view.

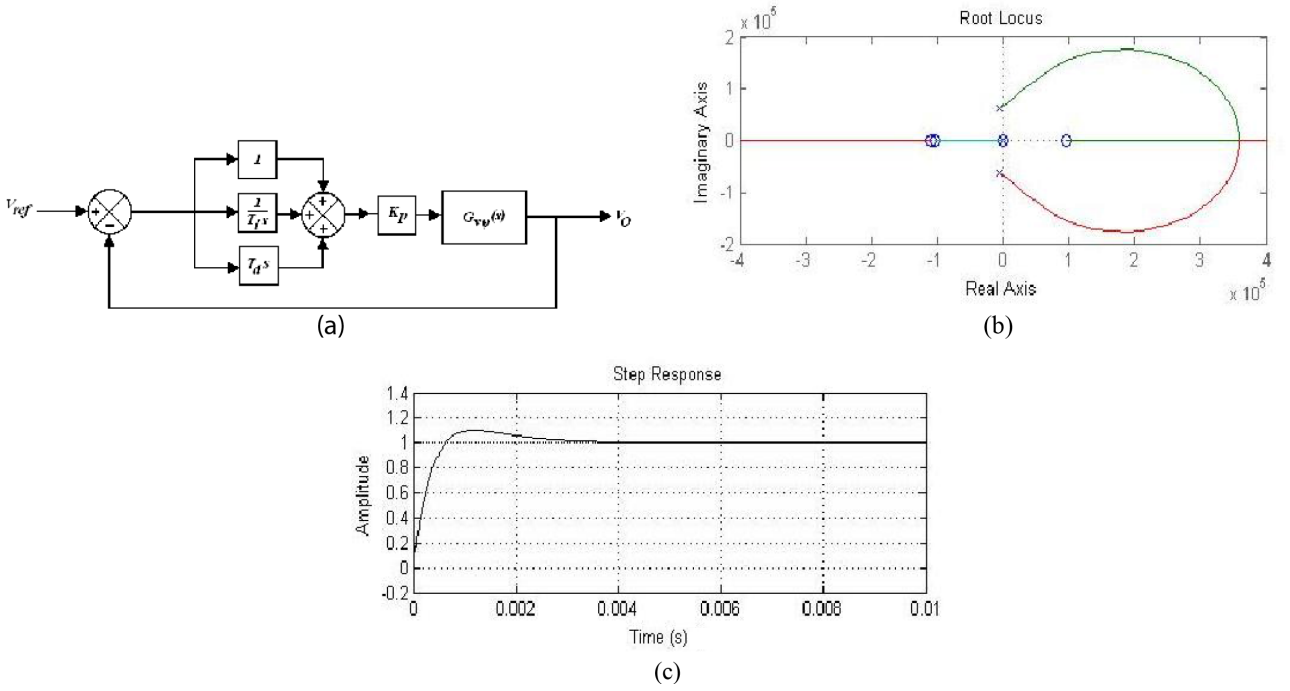

Figure 8. Compensated system response, (a) Bode diagram, (b) Root Locus and (c) unit-step response.

Table 2. Parameters of PID controller.

Proportional gain (K_p)	0.03
Integral time constant (T_i)	1.1×10^{-3} s
Differential time constant (T_d)	9.5×10^{-6} s

5. Simulation and measurement results

5.1. Verification of operation principles

In order to verify the operation principles of the proposed modular isolated bidirectional dc-dc converter, a low power prototype with two modules is implemented as illustrated in Figure 9. The specifications and parameters of the prototype converter are given in Table 3. The converter modular parallel and series bridges are constructed using power MOSFETs (IRFP 250). Two high frequency transformers with turn ratio of 50:50 are connected to the bridges, to transfer the power and perform the galvanic isolation. In addition, an auxiliary inductor is used in series with each transformer to serve as an instantaneous energy storage component. The switching frequency is 20 kHz. Therefore, the modular bridges generate a square wave voltage with a duty ratio of 50% and frequency of 20 kHz. The proposed converter has the capability of bidirectional power flow only by leading or lagging the phase shift between two bridges of the converter. The measurement results for both power flow directions are considered in this section. Thirty-five degrees of phase shift is applied between the two bridges to transfer 110 W from one side to the other side of the converter.

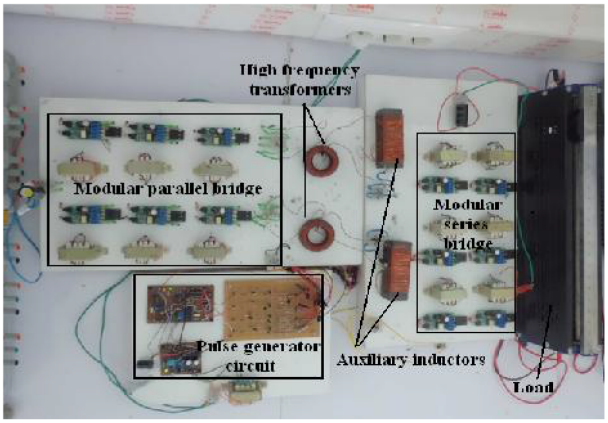

Figure 9. Experimental prototype.

Table 3. Specifications of prototype converter.

Number of modules	2
Input voltage	60 V
Output voltage	120 V
Output power	110 W
Switching frequency	20 kHz
Turn ratio of transformers (n_1:n_2)	50:50
Total leakage inductance	200 μH
Output capacitor	330 μF
Snubber capacitors	150 pF
Input and output bridge switches	IRFP 250

Figure 10 shows the measurement results of the power transmission from parallel bridge to series bridge. Figures 10a and 10b show the primary and secondary square wave voltages of the transformers. The phase shift angle between two square waves is positive. Figures 10c and 10d illustrate the voltage on external inductors and transformer ac currents, which flow through the inductors. The relationship between the inductance voltage and current is perceptible in these figures. The converter measured input dc voltage and input current before the dc filter are shown in Figure 10e, and the converter measured output dc voltage and output current before the dc filter are shown in Figure 10f.

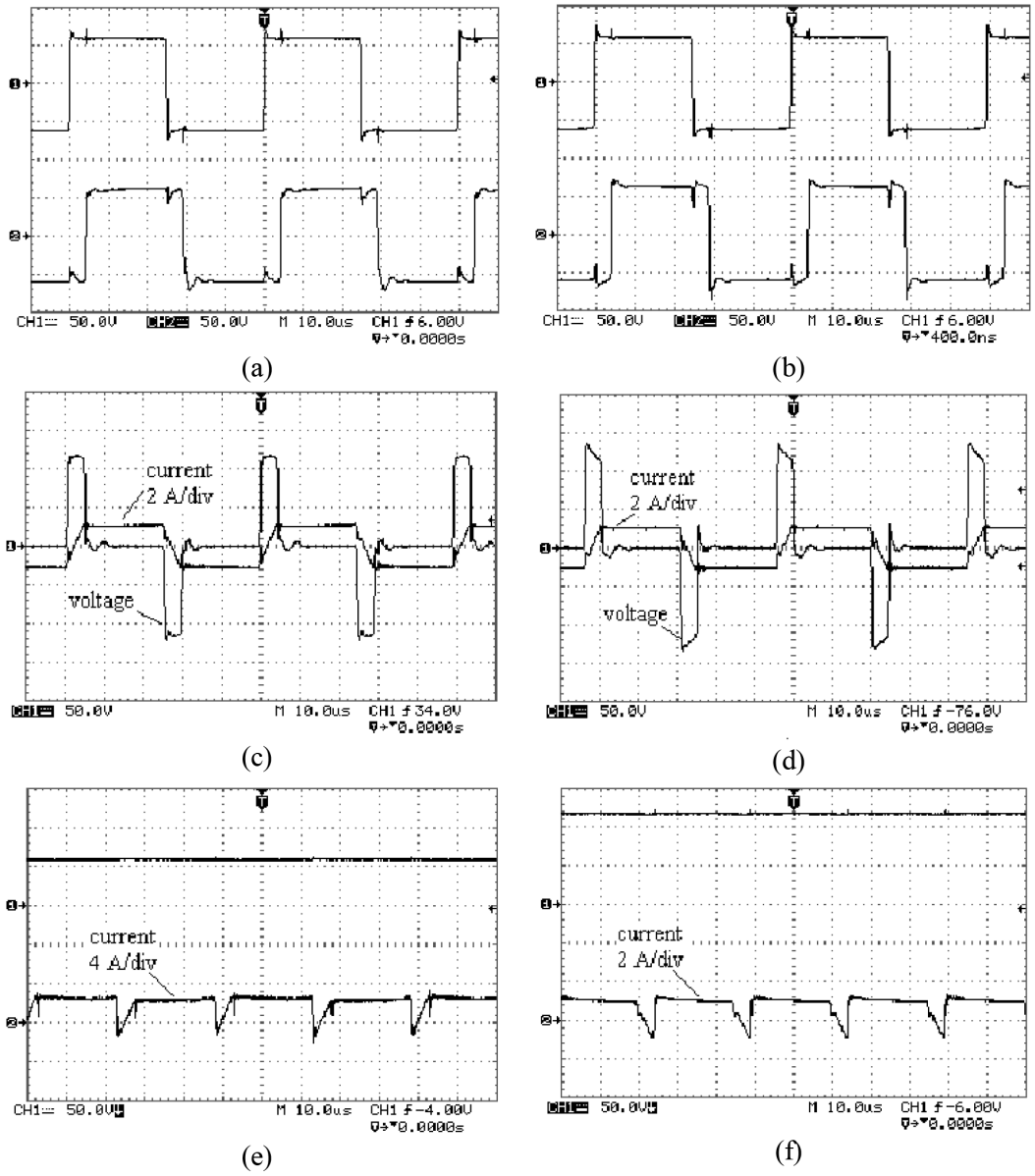

Figure 10. Measurement results of power transmission from parallel bridge to series bridge, (a) and (b) primary (CH1) and secondary (CH2) square wave voltages of transformers, (c) and (d) external inductors voltage and current in both modules, (e) input dc voltage (CH1) and input current, before dc filter, (CH2) and (f) output dc voltage (CH1) and output current, before dc filter, (CH2).

Figure 11a shows the relation between the outer switch current and voltage in the parallel bridge. As this figure indicates, when the current changes its polarity, the voltage on the switch is zero; therefore, the switch is turned on in ZVS condition. Figure 11b illustrates the current and voltage of the inner switch in the modular parallel bridge. ZVS takes place at turn on instant as well. In both switches, when the current starts to decay to zero, the voltage is zero, and when the current reaches zero, the voltage reaches its clamping value. This condition warrants ZVS turn off of these switches. As these figures show, the current in the inner switch is twice that of the outer one in the modular parallel bridge. Figure 11c shows the relation between the current and voltage of the outer switch in the series bridge. The inner switch current and voltage in this bridge are shown in Figure 11d. As these figures illustrate, when the current starts to increase, the voltage on the switch is zero; therefore, the switches are turned on in ZVS condition. Moreover, in both switches, when the current changes its polarity, the switch voltages are zero as well; thus the switches are turned off in ZVS condition. As expected in the series bridge, the inner switch reverse-voltage is twice that of the outer switch reverse-voltage.

Figure 12 shows the measurement results of the reverse direction of power transmission, i.e. from series bridge to parallel bridge. Figures 12a and 12b present primary and secondary square wave voltages of transformers. In this condition, the phase shift angle between two square waves is negative, which means that the primary side phase is lagging the secondary side phase. Figures 12c and 12d show the voltage on external inductors and also transformer ac currents in both modules. Figure 12e shows the converter measured

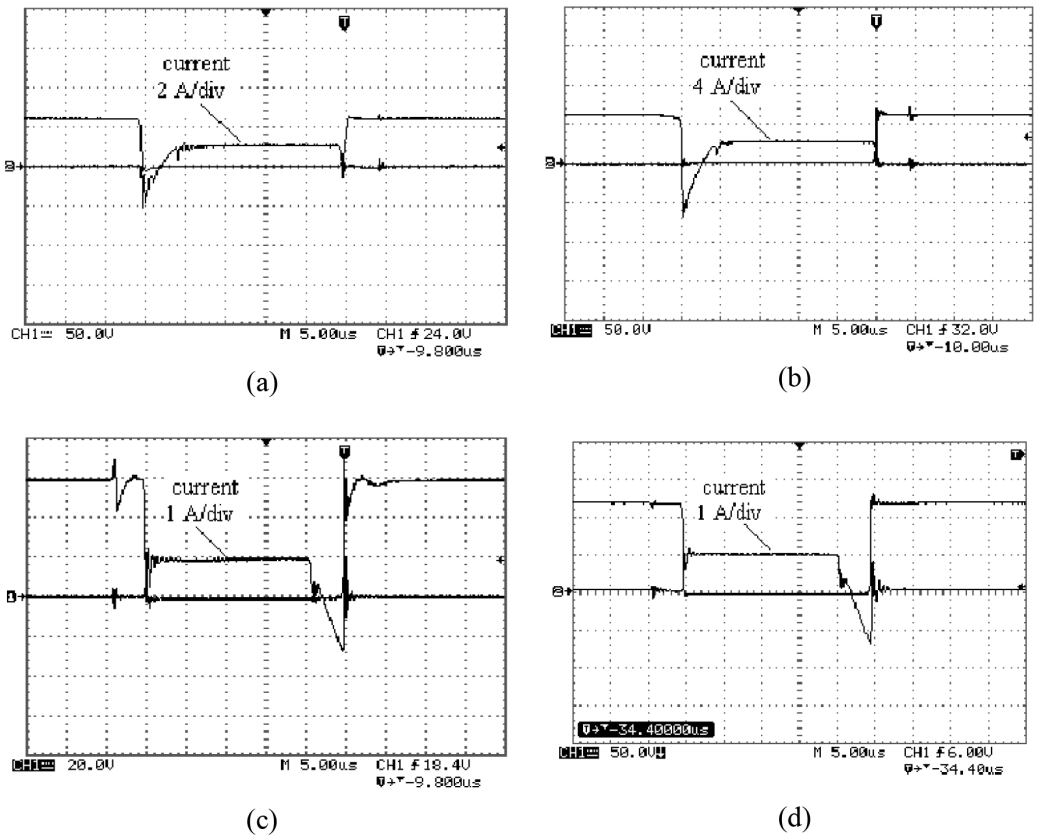

Figure 11. Measurement results of ZVS operation of the proposed converter. ZVS turn on and turn off of (a) outer switches in the modular parallel bridge, (b) inner switches in the modular parallel bridge, (c) outer switches in the modular series bridge, (d) inner switches in the modular series bridge.

input dc voltage and input current before the dc filter, and the converter measured output dc voltage and output current before the dc filter are shown in Figure 12f.

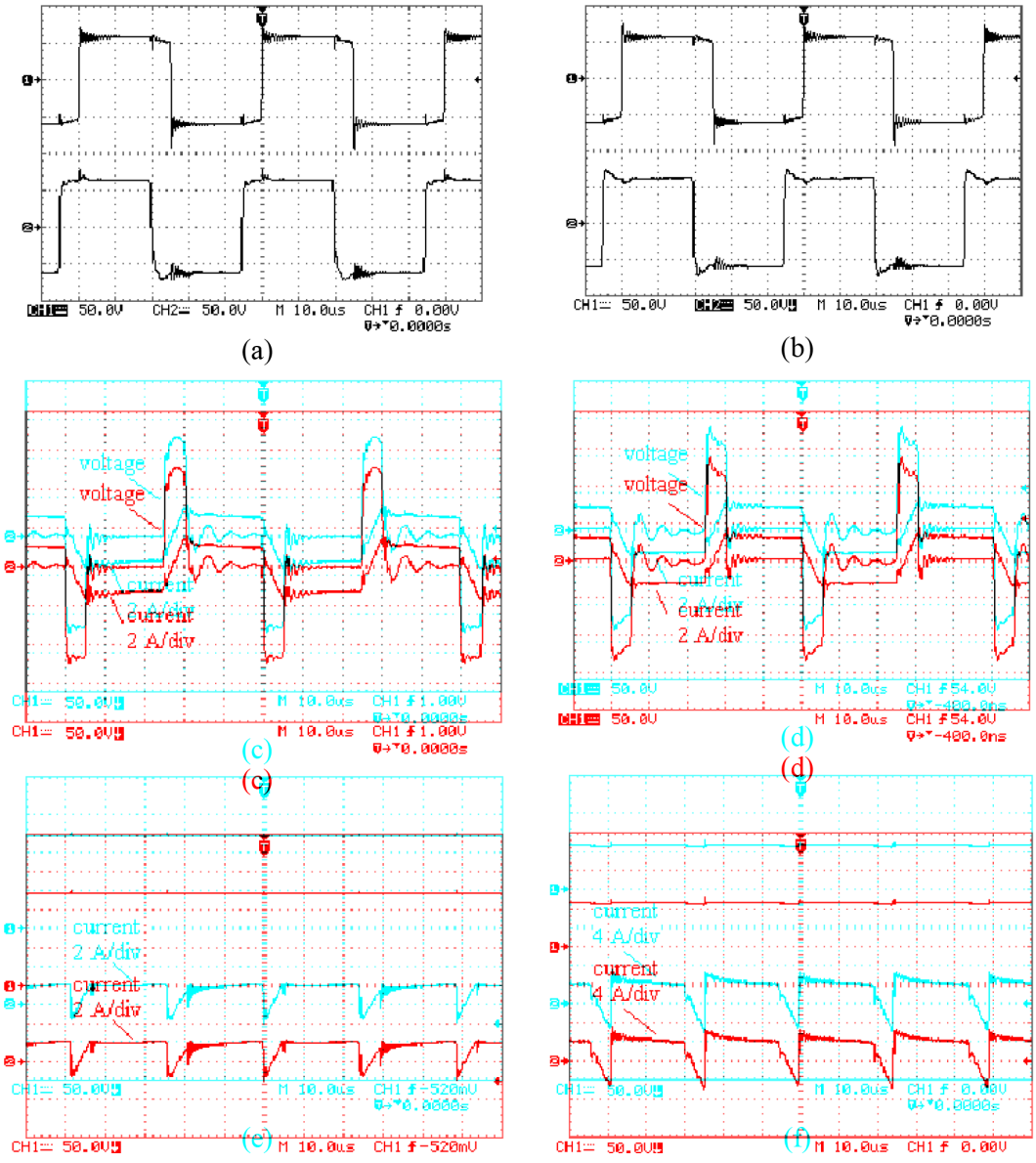

Figure 12. Measurement results of power transmission from series bridge to parallel bridge, (a) and (b) primary (CH1) and secondary (CH2) square wave voltages of transformers, (c) and (d) external inductors voltage and current in both modules, (e) input dc voltage (CH1) and input current, before dc filter, (CH2) and (f) output dc voltage (CH1) and output current, before dc filter, (CH2).

Measurement results confirm operation principles of the experimental prototype for both power flow directions. It is obvious that the proposed converter with more than two modules is useful for high power applications.

5.2. Verification of dynamic performance

The proposed converter extendable configuration and bidirectional power flow capabilities make it suitable as a connection between two dc-links with different nominal voltage for applications such as dc microgrids. Therefore, in this section, closed-loop control of the converter output voltage between two dc-links using PID controller is simulated for step changes in input voltage and load power. The switching model of the proposed converter with two modules is simulated using PSCAD/EMTDC. Simulations are performed for both directions of power flow. Simulation parameters are given in Table 1.

Figure 13 shows simulation results of the power transmission from parallel bridge to series bridge. Two step changes in input voltage and load power values are studied in this simulation. The first disturbance, which is a 20% increase in the input voltage for duration of 0.2 s, starts at $t = 0.2$ s. As shown in Figure 13, the increase in the input voltage results in a decrease in phase shift angle to keep the output power and voltage constant. Therefore, during this disturbance, the load power and voltage remain at their desired values. When the first disturbance ends, the phase shift angle returns to its initial value. The second disturbance is a 20% increase in the load power at time $t = 0.6$ s. As load power increases, the converter phase shift angle increases. Therefore, more power is absorbed from the source, and this leads to an increase in the load current and regulation of the output voltage to its rated value.

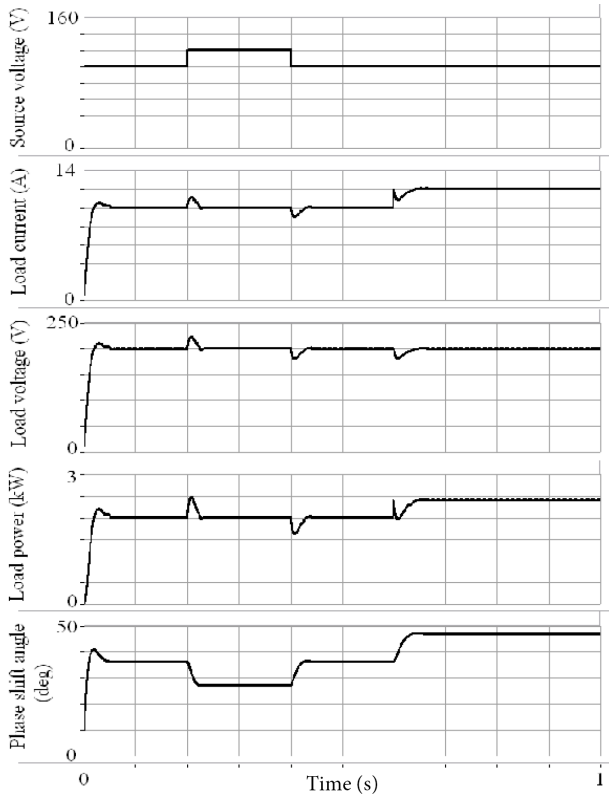

Figure 13. Simulation results of dynamic performance of controlled converter for power transmission, from parallel bridge to series bridge.

Figure 14 shows simulation results of power transmission in reverse direction, i.e. from series bridge to parallel bridge. The effectiveness of the PID controller in the reverse power flow direction is illustrated in this simulation. Notice that the reference voltage and output voltage have been changed for this condition.

Similar to the previous simulation, two step changes in input voltage and load power values are simulated in this simulation. The 20% increase in input voltage starts at $t = 0.2$ s and its duration is 0.2 s. As shown in Figure 14, the increase in input voltage causes a decrease in phase shift angle value to keep the load current and voltage at rated values. Notice that the phase shift angle is negative in this condition. The phase shift angle returns to its initial value, when the voltage step change ends at $t = 0.4$ s. The second step change is a 20% increase in the load power, which occurs at $t = 0.6$ s. As the load power increases, the converter phase shift angle value increases as well. Thus, more power is transmitted from the source to the load, which leads to an increase in the load current and regulation of the output voltage.

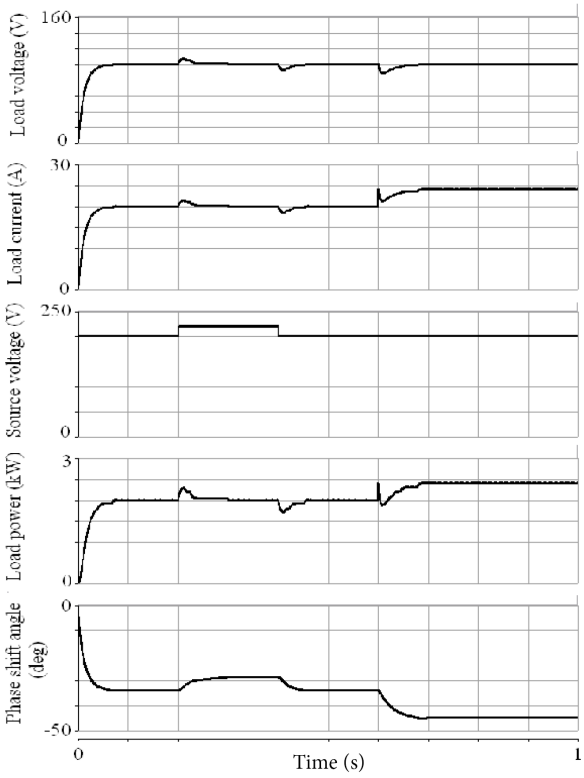

Figure 14. Simulation results of dynamic performance of controlled converter for power transmission, from series bridge to parallel bridge.

These simulation results show the effectiveness of the PID controller for output voltage regulation during dynamic variations at input and output sides of the proposed converter.

6. Conclusion

A new modular isolated bidirectional dc-dc converter has been proposed in this paper. High frequency operation, ZVS capability, and fewer switching devices are the main advantages that make the extended configuration of the proposed converter suitable for high power applications. It has been shown that the proposed converter has the capability of power flow in both directions, only by leading or lagging the phase shift between two bridges. A generalized averaging technique, which represents the averages of state variables using the dc and first order terms of Fourier's series, has been applied to model the proposed converter. The control-to-output transfer function of the converter has been derived using a small-signal average model, and its frequency response,

steady state, and transient responses have been studied. Based on the converter dynamic characteristics, a closed-loop control using a PID controller has been designed. It has been shown that the controller can improve the stability, and obtain acceptable transient and steady state responses. The operation principles of the proposed converter and effectiveness of the PID controller are validated using experimental measurements and simulation results.

References

[1] Ayyanar R, Giri R, Mohan N. Active input–voltage and load–current sharing in input-series and output-parallel connected modular DC–DC converters using dynamic input-voltage reference scheme. IEEE T Power Electron 2004; 19: 1462-1473.

[2] Chen W, Ruan X, Yan H, Tse Ch K. DC/DC conversion systems consisting of multiple converter modules: stability, control, and experimental verifications. IEEE T Power Electron 2009; 24: 1463-1474.

[3] Inoue S, Akagi H. A bidirectional isolated dc-dc converter as a core circuit of the next-generation medium-voltage power conversion system. IEEE T Power Electron 2007; 22: 535-542.

[4] Su GJ, Tang L. A multiphase, modular, bidirectional, triple-voltage dc-dc converter for hybrid and fuel cell vehicle power systems. IEEE T Power Electron 2008; 23: 3035-3046.

[5] Zhou H, Duong T, Sing ST, Khambadkone AM. Interleaved bi-directional dual active bridge DC-DC converter for interfacing ultracapacitor in micro-grid application. IEEE International Symposium on Industrial Electronics; 2010; pp. 2229-2234.

[6] Zhou H, Bhattacharya T, Tran D, Siew T, Khambadkone A. Composite energy storage system involving battery and ultracapacitor with dynamic energy management in microgrid applications. IEEE T Power Electron 2011; 26: 923-930.

[7] Shi J, Gou W, Yuan H, Zhao T, Huang A Q. Research on voltage and power balance control for cascaded modular solid-state transformer. IEEE T Power Electron 2011; 26: 1154-1166.

[8] Fan H, Li H. High-frequency transformer isolated bidirectional DC–DC converter modules with high efficiency over wide load range for 20kVA solid-state transformer. IEEE T Power Electron 2011; 26: 3599-3608.

[9] Ghazanfari A, Hamzeh M, Mokhtari H, Karimi H. Active power management of multihybrid fuel cell/supercapacitor power conversion system in a medium voltage microgrid. IEEE T Smart Grid 2012; 3: 1903-1910.

[10] Shi J, Zhou L, He X. Common-duty-ratio control of input-parallel output-parallel (IPOP) connected DC–DC converter modules with automatic sharing of currents. IEEE T Power Electron 2012; 27: 3277-3291.

[11] Zhao T, Wang G, Bhattacharya S, Huang AQ. Voltage and power balance control for a cascaded H-Bridge converter-based solid-state transformer. IEEE T Power Electron 2013; 28: 1523-1532.

[12] De Doncker R, Divan DM, Kheraluwala MH. A three phase soft-switched high power density dc/dc converter for high power applications. IEEE T Industry Appli. 1991; 27: 63-73.

[13] Kheraluwala MN, Gascoigne RW, Divan DM, Baumann ED. Performance characterization of a high-power dual active bridge DC-to-DC converter. IEEE T Industry Applic 1992; 28: 1294-1301.

[14] Peng FZ, Li H, Su GJ, Lawler JS. A new ZVS bidirectional DC-DC converter for fuel cell and battery application. IEEE T Power Electron 2004; 19: 54-65.

[15] Tao H, Duarte JL, Hendrix MA. Three-port triple-half-bridge bidirectional converter with zero-voltage switching. IEEE T Power Electron 2008; 23: 782-792.

[16] Zhao C, Round S, Kolar J. Full-order averaging modelling of zero-voltage-switching phase-shift bidirectional dc-dc converters. IET Power Electron 2010; 3: 400-410.

[17] Krismer F, Kolar J. Accurate small-signal model for the digital control of an automotive bidirectional dual active bridge. IEEE T Power Electron 2009; 24: 2756-2768.

[18] Bai H, Mi C, Wang C, Gargies S. The dynamic model and hybrid phase-shift control of a dual-active-bridge converter. 34th IEEE Annual Conference on. Industrial Electronics; 2008; pp. 2840-2845.

[19] Jacobs J, Averberg A, Doncker R De. Multi-phase series resonant dc-to-dc converters: Stationary investigations. 36th IEEE Power Electronic Special Conference; 2005; pp. 660-666.

[20] Engel SP, Soltau N, Stagge H, De Doncker W. Dynamic and balanced control of three-phase high-power dual-active bridge DC–DC converters in DC-grid applications. IEEE T Power Electron 2013; 28: 1880-1889.

[21] Erickson RW, Maksimovic D. Fundamentals of Power Electronics, 2nd Edition, New York, NY, USA: Springer, 2001.

[22] Gaviria C, Fossas E, Grino R. Robust controller for a full-bridge rectifier using the IDA approach and GSSA modeling. IEEE T Circuits Systems I: Regular Papers, 2005; 52: 609-616.

[23] Ye Z, Jain P, Sen P. Phasor-domain modeling of resonant inverters for high-frequency ac power distribution systems. IEEE T Power Electron 2009; 24: 911-923.

[24] Qin H, Kimball JW. Generalized average modeling of dual active bridge DC–DC converter. IEEE T Power Electron 2012; 27: 2078-2084.

[25] Qin H. Dual active bridge converters in solid state transformers. PhD, Missouri University of Science and Technology, Rolla, USA, 2012.

[26] Inoue Sh. Akagi Hi. A bidirectional DC–DC converter for an energy storage system with galvanic isolation. IEEE T Power Electron 2007; 22: 2299-2306.

[27] Sanders SR, Noworolski JM, Liu XZ, Verghese GC. Generalized averaging method for power conversion circuits. IEEE T Power Electron 1991; 6: 251-259.

[28] Caliskan VA, Verghese OC, Stankovic AM. Multi frequency averaging of dc/dc converters. IEEE T Power Electron 1999; 14: 124-133.

[29] Ogata K. Modern Control Engineering, fifth edition, Upper Saddle River, NJ, USA: Prentice Hall, 2010.